Article

Micropatterning Chemical Oscillations: Waves, Autofocusing, and Symmetry Breaking

Kyle J. M. Bishop, Marcin Fiakowski, and Bartosz A. Grzybowski

J. Am. Chem. Soc., **2005**, 127 (45), 15943-15948• DOI: 10.1021/ja054851o • Publication Date (Web): 21 October 2005

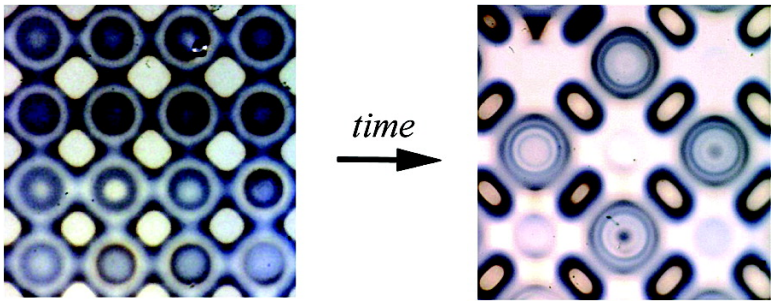

J|A|C|S
ARTICLES
Published on Web 10/21/2005

Micropatterning Chemical Oscillations: Waves, Autofocusing, and Symmetry Breaking

Kyle J. M. Bishop, Marcin Fiałkowski, and Bartosz A. Grzybowski*

Contribution from the Department of Chemical and Biological Engineering and Northwestern Institute for Complexity, Northwestern University, 2145 Sheridan Road, Illinois 60208

Received July 19, 2005; E-mail: grzybor@northwestern.edu

Abstract: Arrays of chemical oscillators are micropatterned by Wet Stamping. The technique is used to demonstrate that chemical waves can be initiated and controlled in oscillatory systems and that such waves can give rise to phenomena not observed in excitable media. Interoscillator coupling and synchronization, kinetic autofocusing, and twist-symmetry breaking are a consequence of the dependence of the oscillation phase on the local concentrations of reagents and on systems' geometry. Conditions under which a generic oscillatory system would exhibit such behaviors are determined.

Introduction

Chemical waves[1−3] (Figure 1), that is, traveling concentration variations in nonlinear chemical systems far from equilibrium, have been widely studied for their relevance to nonlinear and chaotic dynamics,[4,5] biological signaling,[6,7] human health (cardiac,[8] neural[9]) and industrial processes (solid fuel combustion,[10] catalytic oxidation,[11] polymerization[12]). To date, most research has focused on waves traveling through excitable media[13] and initiated from simple geometries;[14−16] in contrast, the propagation of phase-diffusion waves[3,17,18] (cf. Figure 1) in oscillatory systems[19] has been less thoroughly investigated, in part because of experimental difficulties associated with the creation and control of phase gradients necessary to achieve wave propagation. In this work, we (i) introduce an experimental technique based on Wet Stamping (*WETS*)[20−25] that overcomes these limitations and allows patterning of two-dimensional arrays of chemical oscillators and (ii) demonstrate that oscillatory chemical systems not only can emit waves from arbitrary microgeometries but also can give rise to a rich variety of wave behaviors not seen in excitable media: wave acceleration, coupling and synchronization in oscillators arrays, kinetic autofocusing,[26,27] and twist-symmetry breaking.[28,29] These complex phenomena result from the dependence of the oscillation frequency on the local concentrations of chemicals and on the system's geometry. As we show, they can be generalized to all

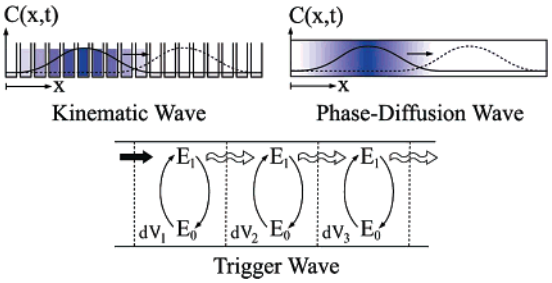

Figure 1. Classification[3] of chemical waves: *Kinematic* and *Phase-diffusion* waves arise from gradients in the oscillation phase between physically isolated and diffusively coupled oscillators, respectively; *Trigger* waves occur in *excitable* media[13] in which small perturbations are amplified ($E_0 \rightarrow E_1$) and then diffuse to perturb neighboring volume elements.

(1) Zaikin, A. N.; Zhabotinsky, A. M. *Nature* **1970**, *225*, 535−538.
(2) *Oscillations and Traveling Waves in Chemical Systems*; Field, R. J., Burger, M., Eds.; John Wiley & Sons: New York, 1985.
(3) Ross, J.; Muller, S. C.; Vidal, C. *Science* **1988**, *240*, 460−465.
(4) Epstein, I. R.; Showalter, K. *J. Phys. Chem.* **1996**, *100*, 13132−13147.
(5) Scott, S. K. *Chemical Chaos*; Oxford University Press: New York, 1991.
(6) Sanderson, M. J.; Charles, A. C.; Boitano, S.; Dirksen, E. R. *Mol. Cell. Endocrinol.* **1994**, *98*, 173−187.
(7) Lee, K. J.; Cox, E. C.; Goldstein, R. E. *Phys. Rev. Lett.* **1996**, *76*, 1174−1177.
(8) Winfree, A. T. *When Time Breaks Down: The Three-Dimensional Dynamics of Electrochemical Waves* and Cardiac Arrhythmias; Princeton University Press: Princeton, NJ, 1987.
(9) Basarsky, T. A.; Duffy, S. N.; Andrew, R. D.; MacVicar, B. A. *J. Neurosci.* **1998**, *18*, 7189−7199.
(10) Matkowsky, B. J.; Sivashinsky, G. I. *SIAM J. Appl. Math.* **1978**, *35*, 465−478.
(11) Ertl, G. *Science* **1991**, *254*, 1750−1755.
(12) Pojman, J. A. *J. Am. Chem. Soc.* **1991**, *113*, 6284−6286.
(13) Winfree, A. T. In *Oscillations and Traveling Waves in Chemical Systems*; Field, R. J., Burger, M., Eds.; John Wiley and Sons: New York, 1985.
(14) Showalter, K.; Noyes, R. M.; Turner, H. *J. Am. Chem. Soc.* **1979**, *101*, 7463−7469.
(15) Foerster, P.; Muller, S. C.; Hess, B. *Proc. Natl. Acad. Sci. U.S.A.* **1989**, *86*, 6831−6834.
(16) Agladze, K.; Keener, J. P.; Muller, S. C.; Panfilov, A. *Science* **1994**, *264*, 1746−1748.
(17) Ortoleva, P.; Ross, J. *J. Chem. Phys.* **1973**, *58*, 5673−5680.
(18) Bodet, J. M.; Ross, J.; Vidal, C. **1987**, *86*, 4418−4424.
(19) Briggs, T. S.; Rauscher, W. C. *J. Chem. Educ.* **1973**, *50*, 496−496.
(20) Fialkowski, M.; Campbell, C. J.; Bensemann, I. T.; Grzybowski, B. A. *Langmuir* **2004**, *20*, 3513−3516.
(21) Bensemann, I. T.; Fialkowski, M.; Klajn, R.; Grzybowski, B. A. *J. Phys. Chem. B* **2004**, *109*, 2774−2778.
(22) Campbell, C. J.; Fialkowski, M.; Klajn, R.; Bensemann, I. T.; Grzybowski, B. A. *Adv. Mater.* **2004**, *16*, 1912−1917.
(23) Klajn, R.; Fialkowski, M.; Bensemann, I. T.; Bitner, A.; Campbell, C. J.; Bishop, K.; Smoukov, S.; Grzybowski, B. A. *Nat. Mater.* **2004**, *3*, 729−735.
(24) Campbell, C. J.; Smoukov, S. K.; Bishop, K. J. M.; Grzybowski, B. A. *Langmuir* **2005**, *21*, 2637−2640.
(25) Smoukov, S. K.; Bishop, K. J. M.; Klajn, R.; Campbell, C. J.; Grzybowski, B. A. *Adv. Mater.* **2005**, *17*, 1361−1365.
(26) Kelley, P. L. *Phys. Rev. Lett.* **1965**, *15*, 1005−1008.
(27) Sutherland, R. L. *Handbook of Nonlinear Optics*; Marcel Dekker: New York, 2003.
(28) Prigogine, I.; Lefever, R.; Goldbeter, A.; Herschkowitz-Kaufman, M. *Nature* **1969**, *223*, 913−916.
(29) Kondepudi, D. K.; Kaufman, R. J.; Singh, N. *Science* **1990**, *250*, 975−976.

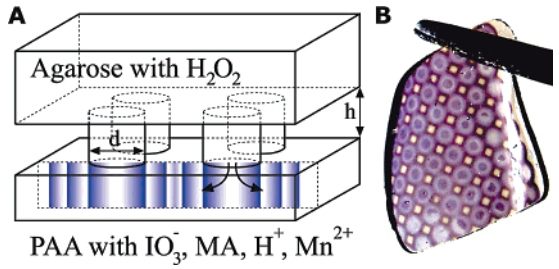

Figure 2. (A) Illustrates the experimental arrangement. (B) Free-standing PAA gel with over 50 active "oscillators" suspended by a pair of tweezers.

oscillating systems that fulfill a set of requirements concerning (i) the functional dependence of the oscillation period on the concentration of a chemical that triggers oscillations and (ii) the relationship between characteristic oscillation and diffusion times. These and other conclusions are supported by numerical simulations as well as generic scaling arguments.

Experimental Section

Our experiments are based on the model Brigg−Rauscher (BR) system[19] whose oscillatory behavior in homogeneous solutions is well documented.[30,31] Most of the chemicals comprising this system (potassium iodate, malonic acid, sulfuric acid, manganese sulfate, thyodene indicator) were contained in a 400-μm-thick film of polyacrylamide (PAA) prepared by polymerizing an aqueous solution of 10% w/v acrylamide (OmniPur 40% w/v acrylamide/bis-acrylamide: 19:1), 0.1% v/v TEMED (1,2-di-(dimethylamino)ethane), 0.07% w/v APS (ammonium persulfate), and 3% w/v thyodene. Prior to use, the PAA sheets were soaked for 1−2 days in an aqueous solution containing 2.15% w/v KIO_3, 0.25% v/v H_2SO_4 (95.6% assay), 0.78% w/v malonic acid (MA), and 0.18% w/v $MnSO_4$. Waves were initiated from the features of a micropatterned agarose stamp[20−25] ($d = 0.5-1$ mm, $h = 0.5$ mm) containing 30% solution of hydrogen peroxide (Figure 2A). The stamp was held in contact with the PAA sheet for 20 s, after which the film was suspended vertically as patterns developed. This arrangement, in which both faces of the gel were exposed to air, was chosen to eliminate the formation of oxygen bubbles, which interfered with controlled wave propagation.

Results and Discussion

(i) BR System. While the stamp is in contact with PAA, H_2O_2 diffuses from the tops of its features into the bulk of the PAA layer. Transport of H_2O_2 is a diffusive process enhanced by the osmotic pressure due to the ionic species contained in PAA.[20] As the peroxide enters the film, it initiates chemical oscillations of the BR system and simultaneously diffuses outward from the stamped features. Coupling between this diffusion and BR oscillations gives rise to chemical waves propagating along the peroxide gradient. In the simplest case of a single, isolated source of waves (Figure 3A), the first wave appears ~30 s after the stamp is applied and propagates radially outward from the feature as a blue band whose color is due to the formation of a complex of $2I_2$, I^-, and thyodene.[32] The velocity of this band decreases with time, suggesting that its propagation is limited by the diffusion of H_2O_2 into the gel. Behind the initial "slow" wave, secondary waves begin to form. These "fast" waves are initiated near the edge of the feature, propagate through the gel, decelerate as they approached the slow-wave envelope, and ultimately die in its vicinity. Importantly, each subsequent wave travels slightly more rapidly than the preceding one, and the radial locations at which the waves die vary, and sometimes even alternate (Figure 3B; the "fishbone" effect). Up to seven waves are created before the system reaches a final equilibrium state.

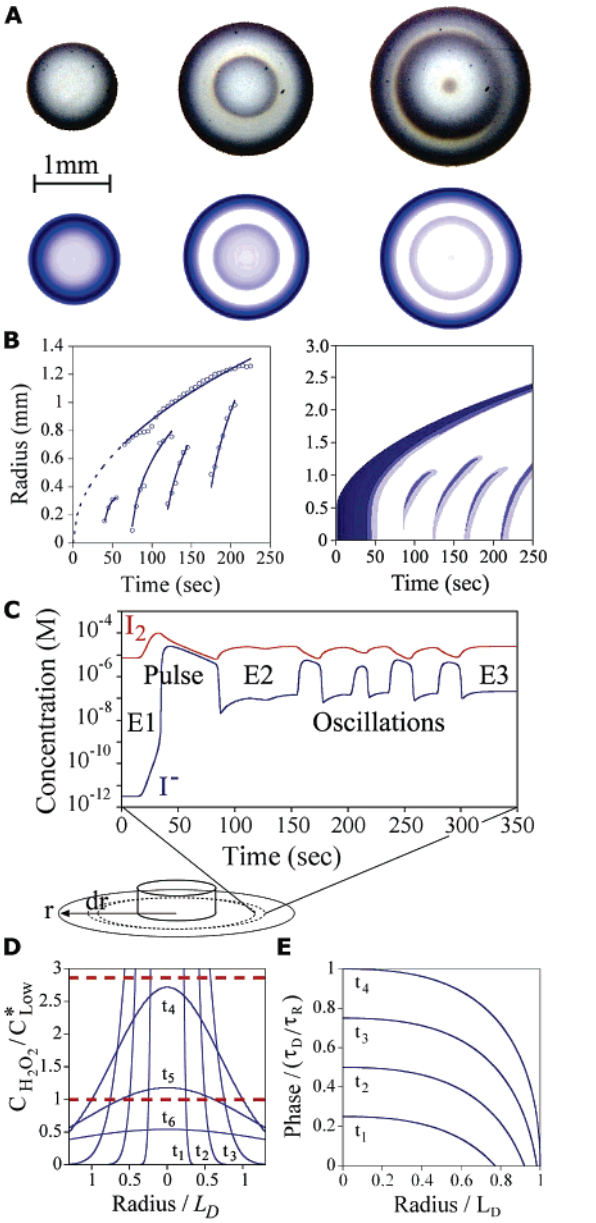

Figure 3. (A) Chemical waves emitted from an isolated, circular feature: experimental images (top) and reaction−diffusion model (bottom). (B) Experimental (left) and simulated (right) trajectories of consecutive waves emanating from a circular feature 1 mm in diameter (the "fishbone effect"). (C) Temporal variations in I^- and I_2 concentrations at a fixed distance from a circular feature as calculated by the one-dimensional RD model (cf. Supporting Information). (D) Calculated concentration profiles (at various times) of peroxide diffusing from a small circular feature. Horizontal dashed lines denote C_{Low}* and C_{Up}*, respectively. (E) Dependence of the scaled oscillation phase $\bar{\phi}(\bar{r},\bar{t})$ on dimensionless radial location $\bar{r}$ and dimensionless time $\bar{t}$ for peroxide *advancing* from a small circular source in the plane (i.e., $\bar{t} \leq 1$).

Modeling (cf. Supporting Information) reproduces the essential features of the experimental system (cf. Figure 3B right) and helps explain the mechanism of the wave formation. In the absence of peroxide, the chemicals in PAA are in a steady,

(30) Dekepper, P.; Epstein, I. R. *J. Am. Chem. Soc.* **1982**, *104*, 49−55.
(31) Noyes, R. M.; Furrow, S. D. *J. Am. Chem. Soc.* **1982**, *104*, 45−48.
(32) Teitelbaum, R. C.; Ruby, S. L.; Marks, T. J. *J. Am. Chem. Soc.* **1978**, *100*, 3215−3217.

equilibrium-like state denoted as *E1* (Figure 3C). Immediately after stamping, the area under the feature has a uniform concentration of H_2O_2 above the upper oscillation limit, C_{Up}* (Figure 3D). When the peroxide diffuses outward, this concentration decreases, and the feature enters the oscillatory regime. Simultaneously, as the front of H_2O_2 propagating from a stamped feature diffuses through the gel, it disrupts the equilibrium-like state *E1*. When the concentration of peroxide at a given location reaches a critical concentration, C_{Pulse}*, the concentrations of intermediates change dramatically over a short period of time before settling into a new, nonoscillatory state *E2* (Figure 3C). Importantly, the *E1* → *E2* transition is accompanied by a spike in the concentrations of I_2 and I^-, giving rise to a burst of blue color. This burst travels with the peroxide front as a radially expanding, blue wave. Behind the first, trigger-like wave (cf. Figure 1), the concentration of H_2O_2 increases steadily, until it reaches the lower threshold value C_{Low}* of the BR oscillatory regime. The closer an element of the gel is to the stamped feature, the sooner it reaches this threshold, and the sooner it starts oscillating. Consequently, a spatial gradient in the phase of oscillation is established, which manifests itself in the propagation of phase-diffusion waves from near the feature's edge toward the expanding peroxide front. As the peroxide pulse continues to spread, the local peroxide concentration eventually falls below C_{Low}* everywhere, leaving the system in a final equilibrium state *E3*.

The velocity of each wave decreases as it propagates outward because the magnitude of the spatial derivative of the oscillation phase, $\partial\phi/\partial r$, increases with distance from the stamped feature, r (cf. Figure 3D,E). To show that, we define a triggering time $t^*(r)$ as the time necessary to bring the concentration of H_2O_2 at location r up to the critical value C_{Low}* required for oscillations. Because the diffusion front of peroxide slows down as r increases, t^* increases faster than linearly with r (Figure 3D); in other words, $dt^*(r)/dr$ is a monotonically increasing function of r. Furthermore, the oscillation phase can be expressed relative to the time at which oscillations were triggered at a given location as $\phi(r,t) = (t - t^*(r))/\tau_{osc}$, in which τ_{osc} is the oscillation period and the effects of phase diffusion[17] are assumed negligible (cf. Supporting Information for details). Since for a stable limit cycle (i.e., $\partial\phi/\partial t =$ constant) the phase is proportional to time, it follows that the velocity of waves, $v = -(\partial\phi/\partial t)/(\partial\phi/\partial r) \propto (dt^*(r)/dr)^{-1}$ decreases with increasing r.

We note that, for simple geometries of the peroxide diffusion front, it is possible to approximate the phase function, $\phi(r,t)$, analytically. For example, in the case of an instantaneous point source (e.g., a small circular feature) diffusing into the surroundings, the axially symmetric concentration profile is given by $\bar{C}(\bar{r},\bar{t}) = \bar{t}^{-1} \exp(-\bar{r}^2/\bar{t})$, where $\bar{t} = t/\tau_D = 4\pi eDC_{Low}^*t/M$, $\bar{r} = r/L_D = \sqrt{M/(\pi eC_{Low}^*)}r$, and $\bar{C} = C/(eC_{Low}^*)$ are dimensionless variables, D is the diffusion coefficient, and M is the total amount of peroxide delivered (moles per unit gel thickness) (cf. Figure 3D). The triggering time $t^*(r)$ is then given by setting the above concentration to the critical value, C_{Low}*, such that $1 = \ln(\bar{t}^*) + \bar{r}^2/\bar{t}^*$ (unfortunately, this equation cannot be solved for $\bar{t}^*$directly). In Figure 3E, the scaled phase function $\bar{\phi}(\bar{r},\bar{t}) = \phi(\bar{r},\bar{t})/(\tau_D/\tau_{osc}) = (\bar{t} - \bar{t}^*(\bar{r}))$ is plotted against $\bar{r}$ for several dimensionless times.

The acceleration of consecutive waves is the result of *phase diffusion*, i.e., the diffusive equilibration of spatial phase gradients (cf. Supporting Information). As diffusion works to erase spatial concentration gradients, the oscillation phase gradients also become more shallow, thereby increasing the wave velocity. The diffusion of phase is also at the heart of the "fishbone" effect (Figure 3B). Since the oscillation period is longer at the peroxide front (defined by $C_{H_2O_2}(r,t) = C_{Low}$*) than behind this front (cf. Figure 5C), then by kinematic arguments alone, one expects subsequent waves to decelerate. In reality, phase diffusion opposes such deceleration and leads to the premature "termination" of waves in "refractory" regions that are still "recovering" from the preceding wave and are not ready to propagate a new one.

The fishbone effect is the first hint of a unique characteristic of wave-emitting oscillatory systems − namely, that in such systems the concentrations of participating chemicals can change local oscillation frequencies and the velocities/modes of wave propagation. As a consequence, the waves behave very differently than those observed in excitable media,[1,33,34] and in some cases give rise to phenomena known from classical optics but never observed in chemical ensembles. We wish to emphasize that these phenomena are not a simple consequence of the diffusion of the triggering reagent, but are ingrained in the system's (nonlinear) chemical kinetics and its geometry, as the following examples illustrate.

When waves are triggered from arrays of proximal (< ∼2 mm apart) features, they influence one another at large separations (roughly an order of magnitude larger than for colliding BZ waves in excitable media[35,36]). This effect manifests itself clearly in arrays of circular BR oscillators (Figure 4A), in which the originally circular waves deform into square ones several hundred micrometers before they actually collide and annihilate. In addition, as the waves approach one another, they accelerate. These effects are explained by the presence of a colorless I_2 front traveling ahead of a visible (i.e., blue) wave due to the $2I_2/I^-$/thyodene complex (cf. Figure 4B). Overlap of counterpropagating I_2 fronts increases the local concentration of I_2 which, in turn, causes an acceleration of the production rate of I^- (the limiting component of the blue complex) and of the oscillation phase, ϕ. Consequently, the velocities of colliding waves increase[37] (cf. Figure 4C), giving the appearance of "remote" sensing.

Oscillators of different sizes emit waves at different frequencies and can influence each other's oscillation phase (Figure 4A, rightmost column, and Figure 4D). This is so because larger oscillators deliver more peroxide than smaller ones, and the concentrations of H_2O_2 behind the triggering fronts they emit are higher than those behind fronts propagating from small oscillators. Since in the BR system the period of oscillation is a convex function of $C_{H_2O_2}$ (i.e., τ_{osc} decreases when $C_{H_2O_2}$ increases above C_{Low}*; Figure 5C), larger oscillators emit waves at a frequency slightly higher than that of the small ones, and wave collisions occur closer and closer to the latter (Figure 4D and Figure S3 in the Supporting Information). Ultimately, the larger ("stronger") emitters completely overpower the smaller ("weaker") ones and set them into antiphase oscillations (Figure

(33) Winfree, A. T. *Sci. Am.* **1974**, *230*, 82−95.
(34) Vanag, V. K.; Epstein, I. R. *Phys. Rev. Lett.* **2003**, 90.
(35) Foerster, P.; Muller, S. C.; Hess, B. *Science* **1988**, *241*, 685−687.
(36) Nagyungvarai, Z.; Muller, S. C.; Hess, B. *Chem. Phys. Lett.* **1989**, *156*, 433−437.
(37) Vanag, V. K.; Epstein, I. R. *Phys. Rev. Lett.* **2001**, *8722*, 228301.

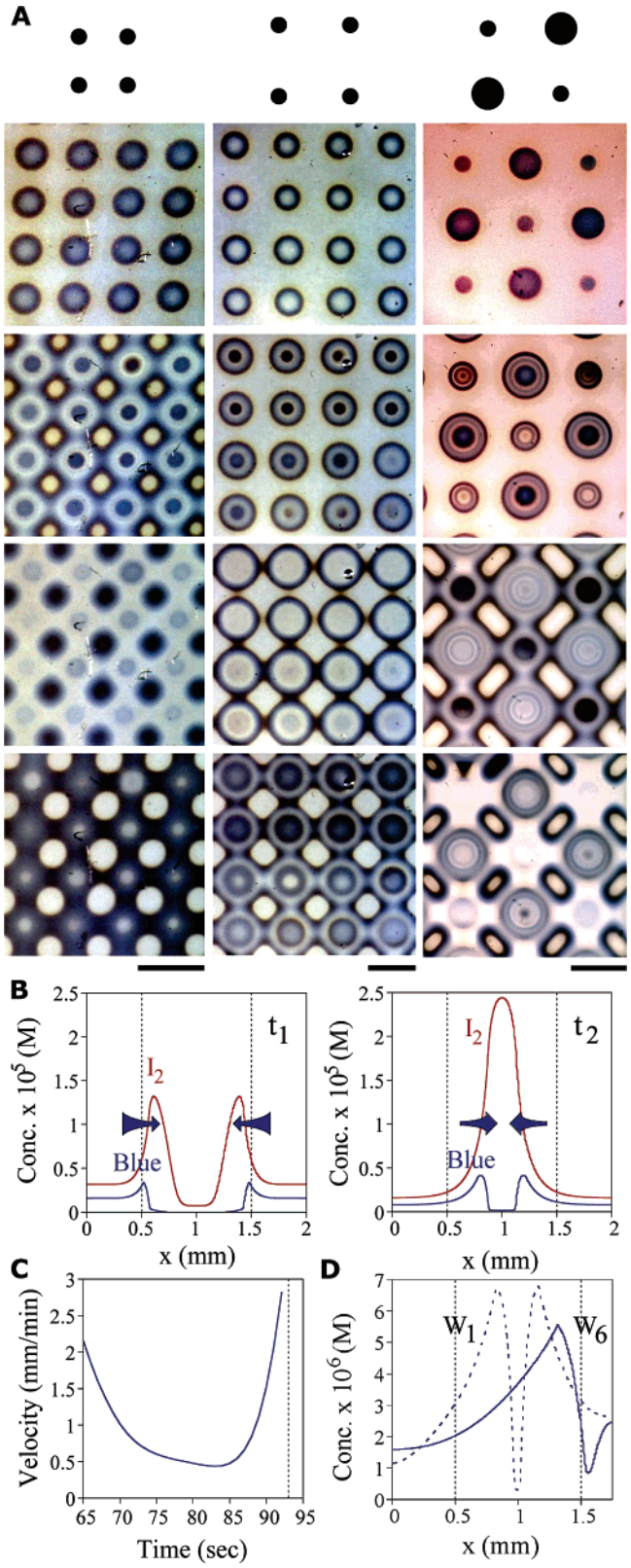

Figure 4. (A) Arrays of wave-emitting chemical oscillators. *Column 1*: 0.5 mm circles separated by 1 mm; *Column 2*: 0.5 mm circles separated by 1.7 mm; *Column 3*: 0.5 mm and 1.0 mm circles separated by 1.5 mm. The times of these images (top to bottom) were approximately 30, 60, 90, and 120 seconds after stamping. (B) Calculated concentration profiles of colliding waves ((blue) $2I_2/I^-$/thyodene complex; (red) I_2). (C) The velocity of colliding wave fronts shown in (B) as a function of time. (D) Wave collisions from oscillators of different sizes (here, 1 mm and 0.5 mm). By the sixth wave (W6), the larger oscillator completely "consumes" the smaller one. See Supporting Information for more details.

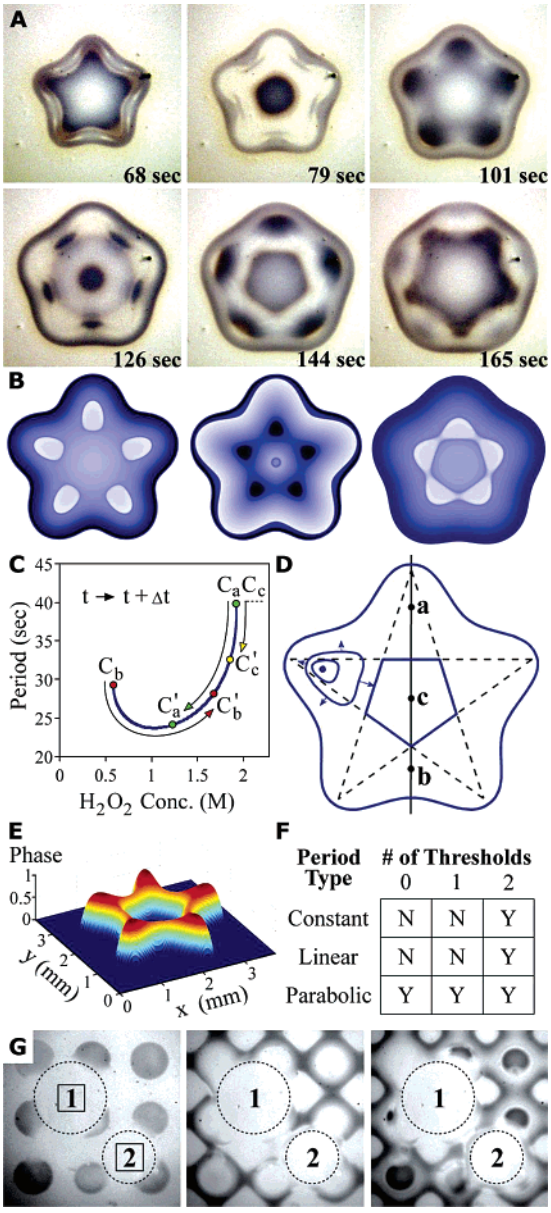

Figure 5. (A) Experimental images of chemical waves initiated from a 3.2 mm (tip-to-tip) pentagonal star. (B) Computer simulations of autofocusing (*left* and *center*) and symmetry-twisting phenomena (*right*). The snapshots correspond, respectively, to 39, 46, and 78 s of the simulation time commensurate with the real (experimental) time (cf. Figure 5A). (C) Calculated dependence of the oscillation period on the concentration of hydrogen peroxide and (D) a schematic diagram of the star-shaped region. (E) Calculated oscillation phase after 30 s of simulation time. The phase is most advanced at the star's tips and lags behind in the corners between the arms and in the center. (F) Summary of the conditions necessary to achieve autofocusing and symmetry-breaking. The other three columns have the numbers of thresholds. (G) Spatially distributed sensing of a 2,6-dihydroxybenzoic acid antioxidant.

4A, rightmost column, and Figure 4D). Interestingly, this process is similar (but not identical) to trigger wave pacemakers in the excitable BZ reagent, in which high frequency pacemakers erode and eventually destroy low-frequency ones.[1]

Most complex wave phenomena emerge when the concentration-period effects couple to the oscillator's geometry. Waves originating from sources whose boundaries have alternating negative and positive curvatures (e.g., starlike) can autofocus into well-defined islands (but, because of phase diffusion, not to infinitesimally small points) and produce "twist" symmetry-

broken patterns. These phenomena are illustrated in Figure 5A, which shows waves propagating from a pentagonal star. The first wave traces the circumference of the entire feature and is continuous. Subsequent waves, however, break into oscillating islands located either near the star's tips or between its edges. These two sets of islands are out of phase with respect to one another, and as one of them appears and grows, the other becomes smaller ("focuses"). In addition, each new wave that now propagates from the feature's center is rotated by 36° with respect to the preceding one, and the rotational symmetry of the overall pattern is reduced from 5-fold to 10-fold. In other words, the system breaks its spatiotemporal symmetry.

The key elements of the focusing and twisting phenomena are (i) oscillations occur only for peroxide concentrations between, C_{Low}* and C_{Up}* and (ii) the oscillation period is a convex function of $C_{H_2O_2}$ (cf. Figure 5C). Initially, the area under the stamped feature has a uniform concentration of H_2O_2 above C_{Up}*. As the peroxide diffuses outward, this concentration decreases and the star enters the oscillatory regime via the upper oscillation threshold. Since the tips of the star (*a* in Figure 5D) lose peroxide more rapidly than the star's center (*c*), these regions oscillate with different periods ($\tau_{osc}(a) < \tau_{osc}(c)$), and the oscillation phase in the center lags behind that near the tips, $\phi_a > \phi_c$. Simultaneously, as the peroxide diffuses outward, the areas between the star's arms successively reach the lower oscillation limit, C_{Low}* and their oscillation phase is advanced with respect to the center, $\phi_b > \phi_c$ (since the period is shorter at *b*). Diffusion also establishes phase gradients between stars' tips and the regions between them: while the former are losing peroxide rapidly, the latter are "flooded" with H_2O_2 supplied from the stars' interior. As a result, the peroxide concentration averaged over the time elapsed since the beginning of the process is lower near the tips than between the arms (cf. Figure 5C) and $\phi_a > \phi_b$. Overall, $\phi_a > \phi_b > \phi_c$ (cf. Figure 5C,E) and the tip regions blink most rapidly as distinct islands, whose periodic shrinkage and expansion is caused by the spatial phase gradients around them. As time passes, the interior of the star enters the oscillating regime (from the direction of the periphery; cf. Figure 5D), and blinking spots expand inward to give characteristic pentagons rotated by 36° with respect to the outer obvolute.

(ii) Genaralization to Other Oscillatory Systems. The phenomena we describe here for the BR system can be generalized to other types of oscillatory reactions. For the waves to be observed at all, (i) there must exist a critical concentration of one or more "trigger" reagents below which no temporal oscillations occur (here, C_{Low}* of peroxide), and (ii) the characteristic diffusion and oscillation times must be such that individual waves can be spatially resolved. To satisfy these conditions, it is necessary that the phase difference between the origin of waves and the triggering front (defined as $r^*(t)$, such that $C(r^*,t) = C_{Low}$*) be greater than unity, $\phi(0,t) - \phi(r^*(t),t) \geq 1$. Equivalently, the characteristic time of diffusion of the triggering front, τ_D, must be greater than the period of oscillation, τ_{osc}. The former quantity can be expressed in terms of the diffusion coefficient, *D*, critical concentration, C_{Low}*, and the total amount, *M*, of the triggering reagent delivered. For the particular case of a triggering pulse emanating from a circular feature, $\tau_D = M/4\pi eDC_{Low}$* (cf. Supporting Information). In the system described here, $\tau_D \approx 30$ s, $\tau_{osc} \approx 40$ s, and $\tau_D/\tau_{osc} \approx 1$, indicating that one wave at a time can be spatially resolved, which agrees with experiments. In general, *n* waves can be resolved behind a triggering front if $\tau_D/\tau_{osc} > n$ (Figure 3E).

To observe frequency coupling in arrays of oscillators of different sizes, the period of oscillation must vary between C_{Low}* and C_{Up}*; only then the oscillator's size affects the frequency of waves it emits. Interestingly, if τ_{osc} were an increasing function of $C_{H_2O_2}$ over the relevant concentration domain, small oscillators would overpower the larger ones, again setting the two into antiphase oscillations.

The minimal conditions for symmetry breaking and autofocusing concern the shape of the oscillator, the functional dependence of τ_{osc} on the trigger's concentration, and the relationship between characteristic times of oscillation and diffusion.

In a series of 2D simulations (cf. Supplemental Information), we verified that these phenomena are not observed in geometries of uniformly positive curvature and without diffusion of the oscillation phase. Moreover, the occurrence of these phenomena depends on the functional dependence of the oscillation period on the trigger concentration (Figure 5F). If there are only one or no oscillation thresholds (either C_{Low}* or C_{Up}*; or none), the oscillation period must be a convex function of the trigger's concentration. With two thresholds (like in the BR system), τ_{osc} can be parabolic, linear, or even a constant function of $C_{H_2O_2}$. It is important to note, however, that nonlinear functions (like the convex one in the BR system) make autofocusing and symmetry-twisting significantly more pronounced/sharper.

Finally, the minimal condition for the breaking of waves into discrete islands (preprequisite for subsequent auto-focusing and symmetry-twisting) is that the oscillation period, τ_{osc}, be smaller than the characteristic diffusion time, τ'_D, after which the diffusing triggering reagent "forgets" its original shape and equalizes phase/concentration gradients along the directions transverse to that of its propagation. For instance, in the case of an *n*-armed regular star oscillator inscribed in a circle of radius *R*, τ'_D can be approximated as $\tau'_D \approx (2\pi R/n)^2/D$. Since it is reasonable to assume that at least two oscillations must be resolved within τ'_D to observe autofocusing, the minimal value of *R* can then be estimated from $\tau'_D(R_{\min}) = 2\tau_{osc}$. For the BR system we studied, $n = 5$, $D = 5 \times 10^{-6}$ cm^2/s, and $\tau_{osc} \approx 40$ s, which gives $R_{\min} \approx 0.5$ mm in very good agreement with experiment. Indeed, we were unable to observe focusing in stars of radii less than 0.5 mm; instead, the resulting patterns were similar to those originating from circular features of similar size.

Conclusions and Outlook

In summary, we demonstrate that systems commonly classified as "oscillatory" can, in fact, give rise to chemical waves and wave phenomena whose characteristics are fundamentally different than those of waves traveling through excitable media. The uniqueness of these waves lies in the fact that their frequency is regulated by local concentrations of chemicals that trigger them. We believe that the patterning technique we developed will enable further study of these effects, using different chemistries, in different geometries, and at different scales. Understanding how concentration gradients influence and control chemical signaling might help explain certain biological processes for which the excitable medium theories are inad-

equate (e.g., vertebrate segmentation,[38,39] cellular pacemaking,[40] and glycolysis[41]). On the practical level, we envision the arrays of micropatterned chemical oscillators to be useful in sensitive (because of inherent chemical nonlinearities), spatially distributed detection schemes, in which the mode and/or extent of wave propagation would provide a visual readout of the amounts and locations of analytes. A simple demonstration of this idea is shown in Figure 5G, where the delivery of small amounts of a 2,6-dihydroxybenzoic acid antioxidant from 1 mm agarose cubes to the gel (prior to stamping the oscillators) disrupts regular BR patterns. Because antioxidants scavenge free radials necessary for oscillations,[42] there are no waves in the regions influenced by the cubes. Importantly, region "1" affected by a cube carrying 0.01 M solution of the oxidant is approximately two times larger than region "2" affected by a 0.005 M cube thus suggesting the quantitative potential of this approach.

(38) Palmeirim, I.; Henrique, D.; IshHorowicz, D.; Pourquie, O. *Cell* **1997**, *91*, 639−648.
(39) Kaern, M.; Menzinger, M.; Hunding, A. *Biophys. Chem.* **2000**, *87*, 121−126.
(40) van Helden, D. F.; Imtiaz, M. S. *J. Physiol. (London)* **2003**, *548*, 271−296.
(41) Muller, S. C.; Mair, T.; Steinbock, O. *Biophys. Chem.* **1998**, *72*, 37−47.
(42) Cervellati, R.; Honer, K.; Furrow, S. D.; Neddens, C.; Costa, S. *Helv. Chim. Acta* **2001**, *84*, 3533−3547.

Supporting Information Available: Supporting Information provides details on the following: (i) the mechanism of BR oscillations; (ii) the importance of the "aging" reaction; (iii) computational modeling; (iv) a generic phase-diffusion model; (v) scaling arguments; (vi) the effects of phase diffusion; (vii) coupling between oscillators of different sizes. This material is available free of charge via the Internet at http://pubs.acs.org.

Acknowledgment. B.A.G. gratefully acknowledges financial support from the Camille and Henry Dreyfus New Faculty Awards Program and the National Science Foundation (Grant No. 0503673). K.B. was supported in part by the NSF-IGERT program "Dynamics of Complex Systems in Science and Engineering" (DGE-9987577).

JA054851O